Measurements of total and positronium formation cross sections for positrons and electrons scattered by hydrogen atoms and molecules

S. Zhou, H. Li, W. E. Kauppila, C. K. Kwan, and T. S. Stein
Department of Physics and Astronomy, Wayne State University, Detroit, Michigan 48202
(Received 12 August 1996)

We have measured total (Q_T) and positronium formation (Q_{Ps}) cross sections for 1–302-eV positrons (e^+'s) and Q_T's for electrons (e^-'s) scattered by hydrogen atoms and molecules. A beam transmission technique is used to measure Q_T's where the projectile beam passes through a low-temperature scattering cell containing a mixture of hydrogen atoms and molecules generated in an adjacent radio-frequency discharge region. Q_{Ps}'s are measured using the same scattering cell by detecting coincidences of 511-keV annihilation γ rays produced by the decay of para-Ps and by the interaction of ortho-Ps with the walls of the scattering cell in which the Ps is formed. The present e^+-H Q_T's and Q_{Ps}'s agree very well with theoretical calculations. Comparisons of the present e^+ and e^--H Q_T's show a merging to within 20% for energies above 12 eV. [S1050-2947(97)03701-3]

PACS number(s): 34.80.−i, 34.90.+q

I. INTRODUCTION

The scattering of positrons (e^+'s) and electrons (e^-'s) by atomic hydrogen are among the most fundamental atomic collision processes. Since hydrogen is the only atom for which the wave functions are known exactly, e^+ and e^--H collision processes provide an attractive testing ground for scattering theories. Although many different calculations of partial and total scattering cross sections (Q_T's) have been reported for these collision systems, it has only been recently that measurements of some of these cross sections for e^+-H scattering have been made [1–6]. In fact, prior to 1994, there were no direct e^--H Q_T measurements above 12 eV, and no e^+-H Q_T measurements at all. e^+-H positronium (Ps) formation cross section (Q_{Ps}) measurements above 13 eV were made in 1992 [2], and e^+-H ionization cross section measurements were made in 1990 [1]. In addition to the opportunity these collision systems present for making direct comparisons between the scattering of particles and antiparticles from the simplest atom, detailed knowledge of e^--H scattering cross sections is important in research on fusion plasmas and in astrophysics, and interest in e^+-H scattering has been stimulated by a need for partial and total e^+-H cross section information by astrophysicists attempting to understand details of the origin of 511-keV annihilation γ rays which have been observed coming from the direction toward the center of the Milky Way galaxy and from solar flares [7].

We recently reported measurements [5] and then additional preliminary measurements [6] of Q_T's for 2- to 302-eV e^+'s and e^-'s scattered by atomic hydrogen using a beam transmission technique where the e^+ or e^- beam passes through a cooled (150 K) aluminum scattering cell containing a mixture of hydrogen atoms and molecules generated in an adjacent radio-frequency (rf) discharge region. Our group has also made measurements of Q_{Ps}'s for e^+'s scattered by alkali atoms [8,9] by detecting the coincidences of 511-keV annihilation γ rays from a scattering cell. Based on the success of the techniques we developed in these previous experiments, it is quite natural for us to combine the two techniques to measure Q_{Ps}'s for e^+-H scattering. In this paper we report measurements for e^+'s (of Q_T's and Q_{Ps}'s) and for e^-'s (of Q_T's) scattered by atomic and molecular hydrogen. The present e^+-H Q_T's supersede our earlier results [5,6], while the e^--H Q_T results reported earlier [6] as preliminary are now considered to be our completed results.

II. EXPERIMENTAL APPROACH

In these experiments, variable energy e^+ beams (obtained from an annealed 0.004-mm-thick tungsten moderator placed in front of a ^{22}Na e^+ source) whose energy distribution has a full width at half maximum (FWHM) of about 1 eV, or e^-'s (secondary e^-'s from the same moderator) with a FWHM of several eV, are guided by a lens system and a curved solenoid [10] to the scattering cell shown in Fig. 1 (as set up for Q_{Ps} measurements). The projectiles which emerge from the cell are detected by a channeltron electron multiplier (CEM) which is off axis for the Q_T measurements [5] and on axis

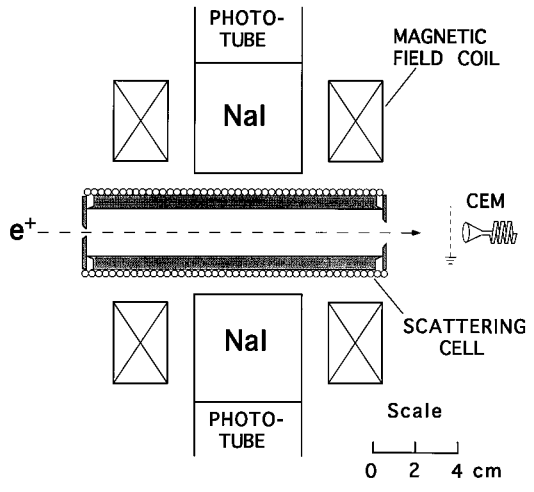

FIG. 1. Experimental setup for Ps formation cross-section measurements.

for the Q_{Ps} measurements. A retarding potential grid assembly located between the scattering cell and the CEM is used to energy analyze the projectile beams and to provide additional discrimination (beyond geometrical considerations) against projectiles scattered through small angles [10]. The target gas flows into the cylindrical aluminum scattering cell from an adjacent Pyrex rf discharge tube. The discharge is excited by feeding about 25 W of rf at 29 MHz into a resonant coaxial cavity. The gas flowing into the scattering cell is H_2 when the rf discharge is off and a mixture of H_2 and H when the rf discharge is on. Recombination of H atoms in the scattering cell is minimized [11] by maintaining the cell temperature at about 150 K. Since the earlier measurements [5] were made in our atomic hydrogen system, the degree of dissociation of the H_2 in the scattering cell has been improved (mainly by using better cleaning procedures for the Pyrex discharge tube) and the precision of the knowledge of that degree of dissociation has also been improved by measuring not only the degree of dissociation of the H_2 effusing from the exit aperture of the scattering cell (which could only be used to set a lower limit on the degree of dissociation in the scattering cell for our initial measurements), but also by measuring the degree of dissociation of the H_2 effusing directly from the rf discharge region and finding that both of these measurements yielded essentially the same result, implying that these measurements both provide the actual degree of dissociation in the scattering cell itself. Thus the amount of recombination of hydrogen atoms to form molecular hydrogen occurring in the scattering cell is negligible, and the fraction of the total number of particles in the scattering cell which are hydrogen atoms can be obtained as a definite number (which for the present results is typically 80%) simply by monitoring the gas effusing from the exit aperture of the scattering cell with a quadrupole mass spectrometer.

A. Total cross-section measurements

In our total cross-section experiment, we use a beam transmission technique [5] to measure Q_T's where the e^+ (or e^-) beam is passed through the scattering cell. We first measure relative total cross sections for $e^+(e^-)$-H_2 scattering with the rf discharge turned off. These are relative cross sections because they are obtained using the pressure measured (using a capacitance manometer) above the rf discharge tube, whereas the pressure is lower than this in the scattering cell [5]. However, by determining the factor required to normalize our relative $e^+(e^-)$-H_2 cross section at 100 eV to our corresponding earlier absolute $e^+(e^-)$-H_2 Q_T measurement [12] and applying this same factor to all of our relative $e^+(e^-)$-H_2 Q_T measurements, we are able to obtain absolute total cross sections, $Q_T(H_2)$ for $e^+(e^-)$-H_2 scattering, and these values are in turn used to obtain our absolute total cross sections, $Q_T(H)$ for $e^+(e^-)$-H scattering.

In order to obtain the absolute total cross section $Q_T(H)$ for $e^+(e^-)$'s scattered by atomic hydrogen, we determine the projectile beam attenuation with the rf discharge on $[(N_0/N)_{\text{rf on}}]$ (where N_0 is the number of projectile beam particles transmitted through an evacuated scattering cell of length L, and N is the number transmitted through the same scattering cell when it contains target gas) and the beam attenuation with the rf discharge off $[(N_0/N)_{\text{rf off}}]$ with the flow of H_2 into the discharge tube kept constant. Using this information, $Q_T(H)$ can be determined from the relationship [13]

$$Q_T(H)=\frac{Q_T(H_2)}{\sqrt{2}}\left[\frac{1}{f}\left\{\frac{\ln(N_0/N)_{\text{rf on}}}{\ln(N_0/N)_{\text{rf off}}}-1\right\}+1\right], \quad (1)$$

where $f=1-n'(H_2)/n(H_2)$ is the degree of dissociation of H_2, while $n'(H_2)$ and $n(H_2)$ are the number densities of molecular hydrogen in the scattering cell for the discharge on and off, respectively.

TABLE I. Estimated experimental percentage errors (maximum percentage errors in parentheses) contributing to the present positron- and electron-H total cross-section measurements. In addition, statistical uncertainties (given in Table III), and the effect of the uncertainty in the energy assignment (0.5 eV for both positrons and electrons) and of the energy widths of the positron (1 eV FWHM) and electron (several eV FWHM) beams would have to be combined with the experimental error subtotals to obtain overall errors.

	e^+	e^-
$Q_T(H_2)$	6(17.5)	5(14.5)
N, N_0	2(4)	2(4)
f	5(5)	5(5)
n	3.5(6)	3.5(6)
L	2(2)	2(2)
Subtotal	9.0(34.5)	8.4(31.5)

The estimated experimental errors for our Q_T measurements are summarized in Table I, where the ''experimental errors'' listed represent the combining in quadrature of the errors associated with each measured experimental parameter, while the ''maximum errors'' are the simple addition of each individual error component. A source of error not included in Table I relates to our inability to discriminate against elastic scattering at small forward angles which results in our measured Q_T's being lower than the actual values. The estimated upper limits for the angular discrimination values [10] of this experiment for e^+-H elastic scattering at representative energies (and the resulting estimated amounts by which our Q_T measurements may be too low) are 28° at 4.5 eV (35% too low), 25° at 11 eV (10% too low), 26° at 21 eV (3% too low), and $\leqslant$15° for energies $\geqslant$50 eV ($<$2% too low). Similar estimates for our e^--H measurements are 30° at 2 eV ($\leqslant$5% too low), 9° at 11 eV (5% too low), 5° at 20–50 eV (5% too low), and $\leqslant$4° for energies $\geqslant$100 eV ($<$2% too low). Discrimination of this experiment for e^+ and e^--H inelastic scattering should be complete due to the use of the retarding potential grid located after the scattering cell.

B. Ps formation cross-section measurements

Our experimental approach [8] for measuring Q_{Ps} mainly involves setting a lower limit on Q_{Ps} which is obtained by detecting (with photomultiplier tubes and attached NaI scintillators on opposite sides of the scattering cell as shown in Fig. 1) the 511-keV annihilation γ rays in coincidence produced by the decay of para-Ps formed by e^+-H and e^+-H_2

TABLE II. Estimated experimental percentage errors (maximum percentage errors in parentheses) contributing to the present positron-H, H_2 positronium formation cross-section measurements. In addition, statistical uncertainties (given in Table IV), and the effect of the uncertainty in the positron beam energy assignment (0.5 eV) and of the energy width of the positron beam (1 eV FWHM) would have to be combined with the experimental error subtotals to obtain overall errors.

	H	H_2
$Q_T(H_2)$	0(0.1)	0.3(0.8)
$Q_T(H)$	0.5(2)	
$Q_{Ps}(H_2)$	2(4)	
ϵ_{CEM}	5(5)	5(5)
ϵ_G	5(5)	5(5)
F_G	5(5)	5(5)
f	5(5)	
n	3.5(6)	3.2(5.5)
L	2.6(2.6)	2.6(2.6)
Subtotal	11.1(34.7)	9.6(23.9)

collisions in the scattering cell, and by the interaction of ortho-Ps (which corresponds to $\frac{3}{4}$ of all Ps formed in the cell) with the walls of the cell. An axial magnetic field (90 G) prevents scattered e^+'s from reaching and annihilating on the cell walls and contributing to the coincidence signal, while direct annihilation of e^+'s in the target gas is known to be negligible [14] at the e^+ energies used in the present investigation.

To determine our measured Ps formation cross section $Q_{Ps}(H)$ for e^+'s scattered by atomic hydrogen, we first determine the total and positronium formation cross sections for e^+-H_2 scattering, $Q_T(H_2)$ and $Q_{Ps}(H_2)$ (with the rf discharge off), and the total cross sections for e^+-H scattering, $Q_T(H)$ (with the rf discharge on). Then we measure the coincidence counts of 511-keV γ rays from the scattering region with the rf discharge on when the flow of H_2 into the discharge tube is kept constant. Using this information, $Q_{Ps}(H)$ can be determined (see the Appendix) from the relationship

$$Q_{Ps}(H)=\frac{N_{Ps}\epsilon_{CEM}}{N_0 e^{-aL_s}\epsilon_G F_G^2(1-e^{-aD})}\left[\frac{(1-f)}{\sqrt{2}f}\,Q_T(H_2)+Q_T(H)\right]-\frac{(1-f)}{\sqrt{2}f}\,Q_{Ps}(H_2), \tag{2}$$

where

$$a=\frac{\ln(N_0/N)_{rf\ off}}{L}\left[f\left(\frac{\sqrt{2}Q_T(H)}{Q_T(H_2)}-1\right)+1\right], \tag{3}$$

$$Q_{Ps}(H_2)=\frac{N_{Ps}\epsilon_{CEM}}{N_0 e^{-nQ_T(H_2)L_s}\epsilon_G F_G^2(1-e^{-nQ_T(H_2)D})}\,Q_T(H_2), \tag{4}$$

N_{Ps} is the detected number of 511-keV γ-ray coincidences for the rf discharge on for Eq. (2) and off for Eq. (4), ϵ_{CEM} (=0.80) is the measured efficiency of the CEM for detecting positrons, N_0 is the detected number of primary beam positrons, L is the length of the scattering cell, L_s is the distance along the cell axis from the cell entrance to the leading edge

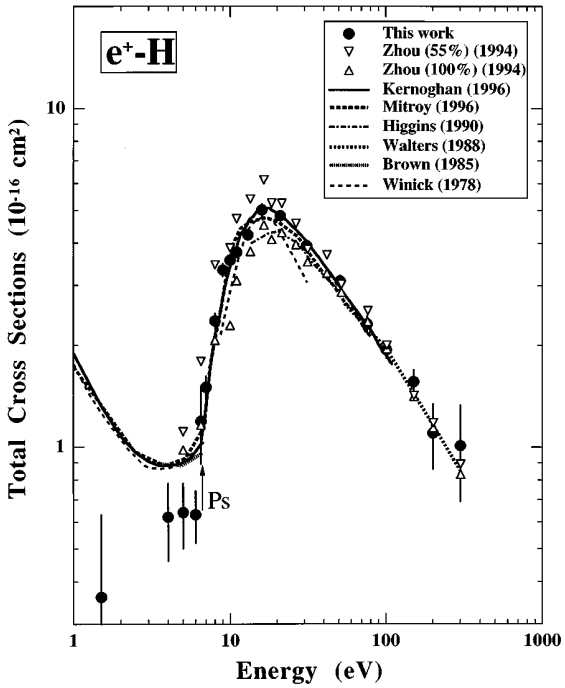

FIG. 2. Total cross sections for positron-H scattering. The arrow indicates the positronium formation threshold. Statistical uncertainties for the present results in this and the following figures are represented by error bars except where they are encompassed by the size of the symbols.

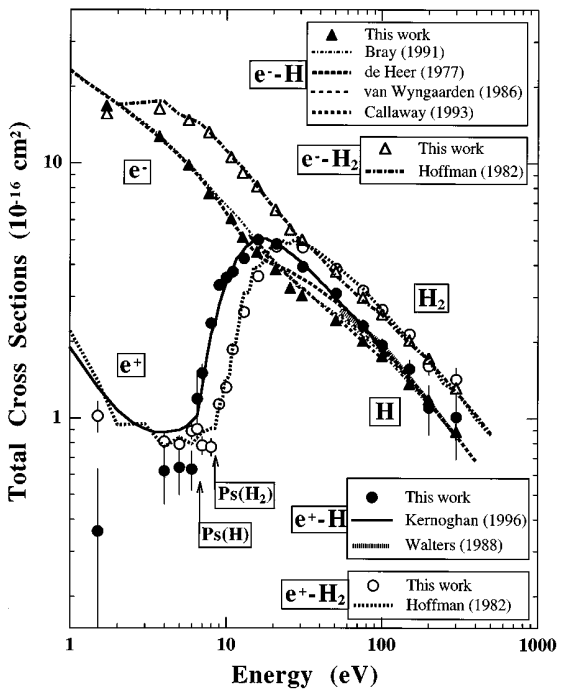

FIG. 3. Comparison of positron- and electron-H and H_2 total cross sections. Arrows indicate the locations of the positronium formation thresholds for H (6.8 eV) and H_2 (8.6 eV).

TABLE III. Present total cross-section results with statistical uncertainties (in units of 10^{-16} cm^2) for $e^{\pm}$-H, H_2 collisions.

E (eV)	e^+-H_2 Q_T	e^+-H Q_T
1.5	1.02±0.14	0.36±0.27
4.0	0.81±0.07	0.62±0.16
5.0	0.79±0.06	0.64±0.14
6.0	0.89±0.06	0.63±0.11
6.5	0.91±0.08	1.19±0.30
7.0	0.78±0.06	1.50±0.12
8.0	0.77±0.06	2.36±0.12
9.0	1.13±0.06	3.33±0.14
10.0	1.32±0.06	3.56±0.15
11.0	1.86±0.05	3.76±0.10
13.0	2.61±0.07	4.23±0.15
16.0	3.61±0.08	5.01±0.21
21.0	4.71±0.06	4.82±0.14
31.0	4.68±0.08	3.93±0.13
51.0	3.86±0.05	3.09±0.12
76.0	3.17±0.07	2.31±0.13
101.0	2.67±0.05	1.94±0.11
151.0	2.14±0.07	1.56±0.13
201.0	1.60±0.12	1.10±0.24
301.0	1.42±0.15	1.01±0.32
E (eV)	e^--H_2 Q_T	e^--H Q_T
1.7	15.66±0.07	16.83±0.17
3.7	16.39±0.05	12.75±0.12
5.7	14.74±0.04	9.84±0.07
7.7	13.24±0.08	7.59±0.17
10.7	10.57±0.03	6.07±0.07
12.7	9.18±0.07	5.12±0.17
15.7	8.10±0.07	4.49±0.13
20.7	6.55±0.02	3.83±0.04
25.7	5.49±0.03	3.25±0.05
30.7	5.01±0.03	3.04±0.05
50.7	3.76±0.04	2.43±0.07
75.7	2.98±0.03	2.01±0.05
100.7	2.56±0.02	1.75±0.04
150.7	2.02±0.02	1.36±0.04
200.7	1.71±0.03	1.18±0.05
300.7	1.31±0.03	0.89±0.06

of the scintillators, D is the diameter of the scintillators, ϵ_G (=0.0055) is the measured efficiency of our system (by using a movable, calibrated ^{22}Na test source) for detecting coincidences of 511-keV γ rays produced in the interior of our scattering cell (ignoring γ-ray absorption by the cell walls), and F_G (=0.87) is the fraction of 511-keV γ rays transmitted through the cell walls. $Q_{\rm Ps}(H_2)$ is determined using the relationship given in Eq. (4). Since $\frac{1}{4}$ of all Ps produced is para-Ps, while $\frac{3}{4}$ is ortho-Ps, ideally $Q_{\rm Ps}$ should equal $4\times Q_{\text{para-Ps}}$. The lifetime of para-Ps is 0.125 ns and of ortho-Ps is 142 ns. The kinetic energy of Ps is essentially equal to the incident positron energy minus the difference between the ionization threshold of the target atom (molecule) and the binding energy of Ps. As a result, in our experiment all of the para-Ps will decay within 1 mm of where it is formed (i.e., near the positron beam axis), while ortho-Ps with its much longer lifetime will generally collide with the cell walls (e.g., with an energy of 1 eV it will travel about 6 cm during its mean lifetime). Since these coincidence measurements should account for all of the para-Ps formation and at least part of the ortho-Ps formation (through the interaction of ortho-Ps with the cell walls), they result in lower limits (LL) on $Q_{\rm Ps}$. The estimated experimental errors for our $Q_{\rm Ps}$ measurements are summarized in Table II.

A second approach [8] to obtain information about $Q_{\rm Ps}$'s is to perform a beam transmission measurement similar to the measurement of Q_T except that deliberate efforts are made (by using no retarding potential on the CEM retarding elements, high axial magnetic fields in the scattering region, and a large cell-exit aperture) to detect all of the scattered positrons except those which have formed Ps and those scattered into the backward hemisphere. This measurement with the angular discrimination deliberately made poor would then be an upper limit on $Q_{\rm Ps}$, which we refer to as UL.

III. RESULTS AND DISCUSSION

A. Total cross sections

Our present e^+-H Q_T measurements are listed in Table III and shown in Fig. 2 along with our original measurements [5] and prior theoretical results [15–21]. There is very good agreement of the present measurements with the coupled-33-state approximation calculation of Kernoghan *et al.* [21] and the 28-state close-coupling approximation calculation of Mitroy [20] (except at the lowest energies of overlap where the discrimination of our experiment against e^+'s scattered elastically through small angles tends to become a more significant problem), and with a pseudostate close-coupling approximation calculation of Walters [16] at higher energies.

The present e^+-H and e^--H Q_T's are compared in Fig. 3 with our prior [12] measured e^+-H_2 and e^--H_2 Q_T's and with prior semiempirical results [22], and theoretical calculations [16,21,23–26]. In addition to the very good agreement between the present measured e^+-H Q_T's with the theoretical calculations, Fig. 3 shows that there is also very good agreement between the present measured e^--H Q_T's and the coupled-channel optical potential calculation of Bray, Konovalov, and McCarthy [23,24]. An additional observation that can be made in Fig. 3 is that the e^+-H and e^--H Q_T's are quite close to each other (within about 20%) from about 12 eV to the highest energies investigated (300 eV). The proximity of the e^+-H and e^--H Q_T's is intriguing, particularly near the low end of the energy range, when it is realized that the integrated elastic cross section for e^-'s is estimated [23] to be more than four times as large as that calculated [15] for e^+'s at 30 eV and still about 40% larger even at 300 eV, while our measured Ps formation cross section (see next section) near 30 eV comprises about 30% of Q_T for e^+-H scattering. This proximity of the e^+-H and e^--H Q_T's suggests that even though the partial cross sections that contribute to Q_T are behaving very differently for e^+'s and e^-'s, the various scattering channels for each projectile appear to be ''coupled'' with each other in the sense that the sums of the partial cross sections (i.e., the Q_T's) for e^+'s and e^-'s turn out to be quite close to each other. It would seem relevant that a theoretical analysis by Dewangan

TABLE IV. Present positronium formation cross-section results with statistical uncertainties (in units of 10^{-16} cm^2) for e^+-H, H_2 collisions.

E (eV)	e^+-H Q_{Ps}	e^+-H Q_{Ps}(LL)
4.0	−0.002±0.044	
5.0	−0.033±0.065	
6.0	0.139±0.058	
7.0	0.568±0.084	0.568±0.084
8.0	1.080±0.094	
9.0	1.680±0.112	1.573±0.104
10.0	1.940±0.110	
11.0	2.355±0.114	2.105±0.101
12.0	2.765±0.115	2.489±0.104
13.0	2.925±0.096	
16.0	2.930±0.077	2.681±0.070
18.5	2.545±0.077	2.260±0.068
21.0	2.275±0.073	1.960±0.063
26.0	1.604±0.070	1.316±0.057
31.0	1.210±0.059	
41.0	0.711±0.060	0.465±0.039
51.0	0.453±0.037	0.248±0.020
76.0	0.207±0.033	
101.0	0.115±0.029	
E (eV)	e^+-H_2 Q_{Ps}(LL)	e^+-H_2 Q_{Ps}(UL)
4.0	0.012±0.040	0.33±0.092
5.0	−0.065±0.027	
6.0	0.013±0.034	
7.0	−0.037±0.033	0.28±0.063
8.0	−0.007±0.029	
9.0	0.088±0.036	0.85±0.075
10.0	0.234±0.038	
11.0	0.565±0.049	1.39±0.070
12.0	0.857±0.053	1.77±0.067
13.0	1.220±0.052	
16.0	2.010±0.053	2.83±0.045
18.5	2.080±0.058	3.02±0.050
21.0	2.030±0.058	3.07±0.048
26.0	1.680±0.062	2.63±0.054
31.0	1.610±0.059	
41.0	1.190±0.067	2.00±0.067
51.0	0.712±0.040	1.39±0.049
76.0	0.271±0.034	
101.0	0.180±0.030	

[27] related to higher-order Born amplitudes calculated in the closure approximation has been shown to imply [28,29] that if e^- exchange can be ignored in the e^- scattering case, and if the closure approximation is valid, then a merging (or near merging) of the e^+- and e^--atom Q_T's can occur at energies considerably lower than the asymptotic energies at which the first Born approximation is valid.

B. Ps formation cross sections

The measured upper and lower limits on Q_{Ps} for e^+-H_2 scattering are listed in Table IV and shown in Fig. 4 along with prior measurements [30–32] and available theoretical

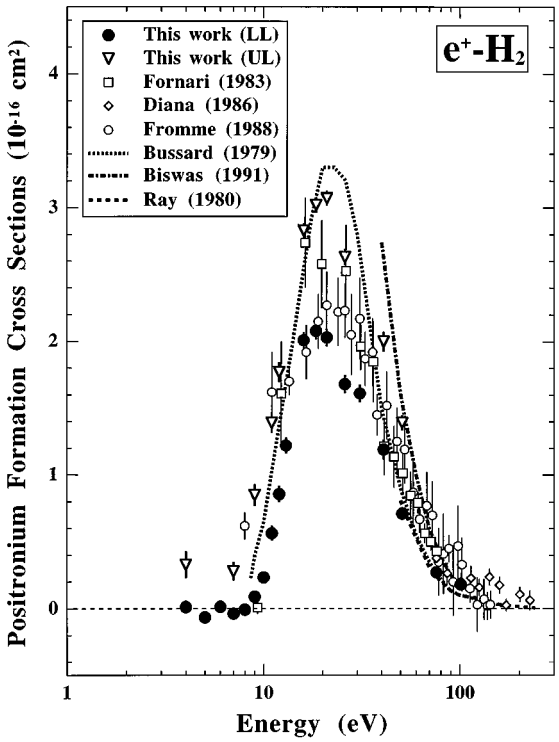

FIG. 4. Positronium formation cross sections for positron-H_2 scattering.

results [7,33,34]. Our measured UL and LL values are within 50% of each other over the energy range from 13 to 30 eV. If there are no serious systematic errors in the measurements, then the true value of Q_{Ps} would be bracketed by these limits. Comparing our present Q_{Ps} measurements with the prior experimental results [30–32], one can see that our UL and LL limits bracket those results quite well. Although our lower limits are obviously on the lower end of all the data, considering that Fornari, Diana, and Coleman [30] and Diana *et al.* [31] measured Q_{Ps} by using basically the same method as our UL approach which actually gives the upper limit of Q_{Ps}, we cannot definitely say which results would be closest to the true values of Q_{Ps}. The theoretical results (using a molecular Jackson-Schiff approximation) of Ray, Ray, and Saha [34] cover only the high-energy tail of Q_{Ps} where they are close to our Q_{Ps}(LL) values, while the semiempirical results of Bussard, Ramaty, and Drachman [7] and first Born approximation ($n=1$ and 2 states of Ps) results of Biswas *et al.* [33] are roughly consistent with the general trends of our experimental results. It is worth noting that the Q_{Ps} lower limit results we measured for e^+-Ar, -K, -Na, and -Rb scattering [8,9] all agree reasonably well with the other Q_{Ps} measurements (for Ar) and theoretical calculations (for K, Na, and Rb). This may suggest that in those experiments (using essentially the same approach and the same type of apparatus as in the present experiment) a major part of the ortho-Ps, which accounts for $\frac{3}{4}$ of all the Ps formed in the cell, interacts with the cell walls and gives rise to the emission of 511-keV annihilation γ rays in coincidence and this in turn could result in our measured Q_{Ps} lower limits for those atoms being close to the true values of Q_{Ps}, which we would expect may also apply to our H_2 measurements.

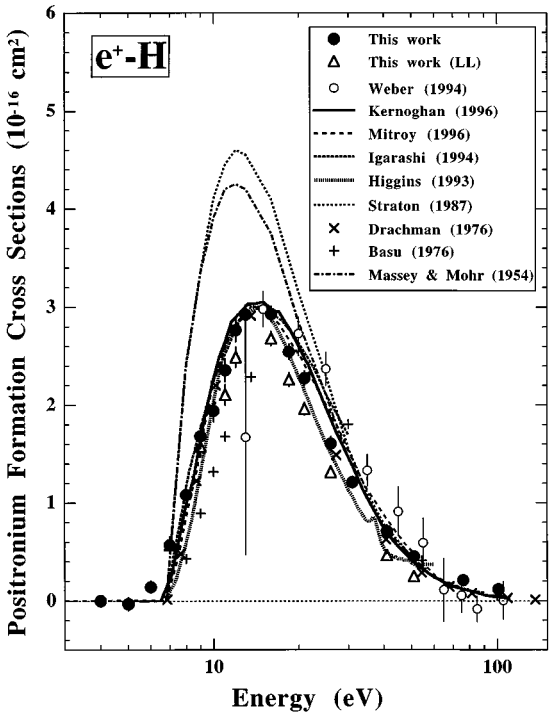

FIG. 5. Positronium formation cross sections for positron-H scattering.

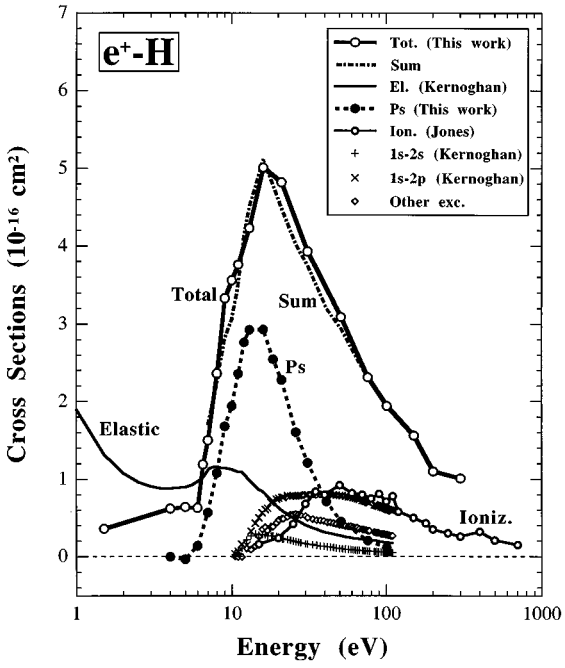

FIG. 6. Total and partial cross sections for positron-H scattering. (Error bars are not shown to improve clarity.)

The measured Q_{Ps}'s for e^+-H scattering are listed in Table IV and shown in Fig. 5 along with prior measurements [3] and some theoretical results [20,21,35–40]. For graphical clarity, and due to limited space, we have selected only a few of the large number of available theoretical calculations considered to be good representations of the most reliable. It should be noticed that our Q_{Ps} results (''This work'') for e^+-H scattering are determined by using our measured lower limit (LL) values of Q_{Ps} for e^+-H_2 scattering in Eq. (2), whereas in order to determine true lower limits of Q_{Ps} [''This work (LL)''] for e^+-H scattering we used our measured upper limit values of Q_{Ps} for e^+-H_2 scattering in Eq. (2). It is to be noted that we have not determined Q_{Ps}(UL) values for e^+-H scattering due to large uncertainties arising from the mixture of H and H_2 in the scattering cell. On the basis of our earlier Q_{Ps} measurements (see discussion above) we expect our ''This work'' results to be the most reliable indicators of the actual Q_{Ps}. Our present Q_{Ps} measurements for e^+-H scattering are seen in Fig. 5 to be reasonably consistent with the prior experimental results [3]. It is very encouraging to see the very good agreement of the present Q_{Ps} measurements with the recent coupled 33-state calculation of Kernoghan *et al.* [21] and the 28-state close-coupling approximation calculation of Mitroy [20], and with most of the other theoretical calculations [35–37]. However, the first Born approximation results of Massey and Mohr [40] and the rather sophisticated Fock-Tani calculation of Straton [38] are about 40–50 % higher than our measurements near the peak region, while the two-state close-coupling approximation calculation results by Basu, Banerji, and Ghosh [39] are lower than our lower limits below 20 eV.

In Fig. 6 we show the relationship of our measured Q_T's (''Total'') and Q_{Ps}'s (''Ps'') to other calculated and measured partial e^+-H cross sections, including the elastic (''Elastic'') and excitation (''1*s*-2*s*,'' ''1*s*-2*p*'') cross sections calculated by Kernoghan *et al.* [21] as well as the ionization cross sections (''Ioniz.'') measured by Jones *et al.* [4]. In addition to these partial cross sections, we have estimated the sum of all of the other discrete excitation cross sections (''Other exc.'') by subtracting the values calculated by Kernoghan *et al.* [21] for all of the above partial cross sections (elastic, 1*s*-2*s*, 1*s*-2*p*, Ps, and ionization) from the Q_T's calculated by Kernoghan *et al.* [21]. If our measured Q_T's and all of the partial cross sections shown in Fig. 6 are correct, then one would expect the sum (''Sum'') of all of those partial cross sections to be equal to our measured Q_T's (''Total''), so Fig. 6 provides a check of the consistency of the partial cross sections shown (including our measured Q_{Ps}'s) and our measured Q_T's. At low energies (below 10 eV), the positron beam energy uncertainty and width and the errors in our Q_T measurements due to the angular discrimination of our experiment result in relatively large experimental errors in our Q_T's and Q_{Ps}'s so a comparison of the ''Sum'' curve and the ''Total'' curve is not too meaningful at such low energies. From 10 to 100 eV, this comparison provides a more stringent consistency check and it is found that the ''Sum'' curve is very close to the ''Total'' curve. The proximity of these curves suggests that the partial cross sections shown in Fig. 6 are consistent with our measured Q_T's, and the consistency of all of these results with each other attaches somewhat more credibility to all of them than would just a comparison of the individual partial cross sections with corresponding calculations or measurements. It should be noted that in order to optimize the clarity of Fig. 6, we have selected only one set of experimental or theoretical results for each of the partial cross sections shown rather than showing several different sets of available results for each partial cross section, and there are other sets of measured or calculated partial cross sections (e.g., the Q_{Ps}'s and or the Q_{ion}'s measured by Weber *et al.* [3]) that could be

substituted for those used in Fig. 6 without perturbing the indicated degree of consistency appreciably. It appears that considerable progress has been made both experimentally and theoretically in understanding this most fundamental atomic collision system, but it still remains that there are no direct measurements of elastic and excitation cross sections for e^+-H scattering.

In addition to using Fig. 6 to check consistency of the e^+-H partial and total cross sections, it is also of interest just to see the relative roles of the various partial cross sections that contribute to Q_T. Between 10 and 35 eV, Ps formation is the largest of all the partial cross sections that contribute to Q_T, reaching a maximum value near 15 eV which is more than three times as large as the elastic cross section at 15 eV which is the next largest partial cross section at that energy, and more than three times as large as the maximum reached by the ionization cross section (near 50 eV). $Q_{\rm Ps}$ at its maximum (near 15 eV) accounts for approximately 60% of Q_T. It is noteworthy that elastic scattering accounts for less than one-fifth of Q_T in e^+-H scattering at and above 15 eV, whereas in the e^--H scattering case it is estimated [41] to account for more than 80% of Q_T at 15 eV and still constitute about 60% of Q_T at 30 eV.

Returning to the indications that our measured e^+-H $Q_{\rm Ps}$'s shown in Figs. 5 and 6 may be close to correct, leads to a consideration somewhat tangent to the main thrust of these investigations, but nonetheless interesting. Since our e^+-H $Q_{\rm Ps}$'s were obtained by detecting 511-keV annihilation γ rays in coincidence, and the decay of ortho-Ps (which constitutes three-fourths of all the Ps formed in our cell) would not tend to contribute to that signal, the implication is that a major part of the ortho-Ps is giving rise to a two-γ-ray coincidence signal upon interacting with the walls of our aluminum scattering cell. Furthermore, this conversion process is occurring efficiently over the entire energy range investigated in our experiments, which includes Ps energies down to just a few eV or less. This observation is consistent with the high degree of ortho-Ps conversion (to a two-γ-ray coincidence signal) suggested by our prior $Q_{\rm Ps}$ measurements for Na, K, Rb, and Ar [8,9]. In contrast, ortho-Ps interacting with a MgO coated surface has been found [42] to have a very low probability of giving rise to a two-γ-ray coincidence signal at low Ps energies (3 eV). Therefore it may be interesting to study this conversion process as a function of Ps energy on various surfaces.

ACKNOWLEDGMENTS

We would like to acknowledge Dr. R. G. H. Robertson for providing valuable information pertaining to the use of a low-temperature aluminum cell for minimizing recombination of atomic hydrogen, Dr. K. Beard for bringing Dr. Robertson's work to our attention, and Dr. M. G. Stewart for equipment used for the present $Q_{\rm Ps}$ measurements. This work is supported by NSF Grant No. PHY 94-22271.

APPENDIX: DETERMINATION OF $Q_{\rm Ps}$(H)

The derivation of Eq. (2) for determining $Q_{\rm Ps}$(H) for e^+-H scattering begins with the basic expression for the attenuation of $\mathcal{N}_0$ projectile beam particles as they pass through a gas scattering region composed of a mixture of H and H_2 (with number densities of n_1 and n_2, respectively),

$$\mathcal{N}(x)=\mathcal{N}_0 e^{-ax}, \tag{A1}$$

where

$$a=n_1 Q_T(\mathrm{H})+n_2 Q_T(\mathrm{H_2}) \tag{A2}$$

and Q_T(H) and $Q_T(H_2)$ are the total cross sections for positrons scattering from H and H_2.

The number of incident positrons that will form Ps in the scattering cell between the NaI scintillators will be

$$\mathcal{N}_{\rm Ps}=\int_{L_s}^{L_s+D}\mathcal{N}(x)[n_1 Q_{\rm Ps}(\mathrm{H})+n_2 Q_{\rm Ps}(\mathrm{H_2})]dx, \tag{A3}$$

where L_s and L_s+D are the distances along the positron beam from the entrance aperture of the cell to where the scintillators (having a diameter D) begin and end, and $Q_{\rm Ps}(H_2)$ is the Ps formation cross section for e^+-H_2 scattering. Integrating Eq. (A3) gives

$$\mathcal{N}_{\rm Ps}=[n_1 Q_{\rm Ps}(\mathrm{H})+n_2 Q_{\rm Ps}(\mathrm{H_2})]\,\frac{\mathcal{N}_0 e^{-aL_s}[1-e^{-aD}]}{a}. \tag{A4}$$

From this expression we obtain

$$Q_{\rm Ps}(\mathrm{H})=\frac{a\mathcal{N}_{\rm Ps}}{n_1\mathcal{N}_0 e^{-aL_s}[1-e^{-aD}]}-\frac{n_2}{n_1}\,Q_{\rm Ps}(\mathrm{H_2}). \tag{A5}$$

Using conditions of constant flow of gas into the scattering cell when the rf discharge tube is on and off, the degree of dissociation of H_2 in the scattering cell is

$$f=1-\frac{n_2}{n_2'}, \tag{A6}$$

where n_2' is the number density of H_2 when the rf discharge is off. The number density of H in the cell when the rf discharge is on is given by

$$n_1=\sqrt{2}fn_2', \tag{A7}$$

where it is recognized that each H_2 produces 2 H atoms and the velocity of H is larger than that of H_2 by $\sqrt{2}$, which increases the pumping speed of the cell-exit apertures for H relative to H_2 by the same factor. The ratio of the number densities of H_2 and H with the rf discharge on is given by

$$\frac{n_2}{n_1}=\frac{1-f}{\sqrt{2}f}. \tag{A8}$$

Considering that when the rf discharge is off the attenuation of the projectile beam in the cell (length L) is

$$\left(\frac{N}{N_0}\right)_{\rm rf\ off}=e^{-n_2' Q_T(\mathrm{H_2})L}, \tag{A8$'$}$$

the expression for a in Eq. (A2) can be rewritten as

$$a=\frac{\ln(N_0/N)_{\rm rf\ off}}{L}\left[f\left(\frac{\sqrt{2}Q_T(\mathrm{H})}{Q_T(\mathrm{H_2})}-1\right)+1\right]. \tag{A9}$$

In this experiment our measured number of primary beam particles N_0 and Ps formation coincidence signal N_{Ps} are related to the actual quantities $\mathcal{N}_0$ and $\mathcal{N}_{\mathrm{Ps}}$ by the expressions

$$\mathcal{N}_0 = N_0 / \epsilon_{\mathrm{CEM}} \tag{A10}$$

and

$$\mathcal{N}_{\mathrm{Ps}} = N_{\mathrm{Ps}} / (\epsilon_G F_G^2), \tag{A11}$$

where ϵ_{CEM} is the measured channeltron detection efficiency for positrons, ϵ_G is the measured efficiency of our system for detecting coincidences of 511-keV γ rays produced in the interior of our scattering cell (ignoring γ-ray absorption by the cell walls), and F_G is the fraction of 511-keV γ rays transmitted through the cell walls. The measured quantity N_{Ps} assumes that all of the ortho-Ps that forms in the scattering cell is converted into 511-keV γ rays at the cell walls and this effect has been taken into account in determining ϵ_G.

With the above information it now follows that

$$Q_{\mathrm{Ps}}(\mathrm{H}) = \frac{N_{\mathrm{Ps}} \epsilon_{\mathrm{CEM}}}{N_0 e^{-aL_s} \epsilon_G F_G^2 (1 - e^{-aD})} \left[\frac{(1-f)}{\sqrt{2} f} Q_T(\mathrm{H}_2) + Q_T(\mathrm{H}) \right] - \frac{(1-f)}{\sqrt{2} f} Q_{\mathrm{Ps}}(\mathrm{H}_2), \tag{A12}$$

making it possible to obtain a measured Ps formation cross section for e^+-H scattering based entirely upon measurable quantities.

[1] G. Spicher, B. Olsson, W. Raith, G. Sinapius, and W. Sperber, Phys. Rev. Lett. **64**, 1019 (1990).

[2] W. Sperber, D. Becker, K. G. Lynn, W. Raith, A. Schwab, G. Sinapius, G. Spicher, and M. Weber, Phys. Rev. Lett. **68**, 3690 (1992).

[3] M. Weber, A. Hofmann, W. Raith, W. Sperber, F. Jacobsen, and K. G. Lynn, Hyperfine Interact. **89**, 221 (1994).

[4] G. O. Jones, M. Charlton, J. Slevin, G. Laricchia, A. Kövér, M. R. Poulsen, and S. Nic Chormaic, J. Phys. B **26**, L483 (1993).

[5] S. Zhou, W. E. Kauppila, C. K. Kwan, and T. S. Stein, Phys. Rev. Lett. **72**, 1443 (1994).

[6] T. S. Stein, J. Jiang, W. E. Kauppila, C. K. Kwan, H. Li, A. Surdutovich, and S. Zhou, Can. J. Phys. **74**, 313 (1996).

[7] R. W. Bussard, R. Ramaty, and R. J. Drachman, Astrophys. J. **228**, 928 (1979).

[8] S. Zhou, S. P. Parikh, W. E. Kauppila, C. K. Kwan, D. Lin, A. Surdutovich, and T. S. Stein, Phys. Rev. Lett. **73**, 236 (1994).

[9] A. Surdutovich, J. Jiang, W. E. Kauppila, C. K. Kwan, T. S. Stein, and S. Zhou, Phys. Rev. A **53**, 2861 (1996).

[10] W. E. Kauppila, T. S. Stein, J. H. Smart, M. S. Dababneh, Y. K. Ho, J. P. Downing, and V. Pol, Phys. Rev. A **24**, 725 (1981).

[11] R. G. H. Robertson, T. J. Bowles, J. C. Browne, T. H. Burritt, J. A. Helffrich, D. A. Knapp, M. P. Maley, M. L. Stelts, and J. F. Wilkerson, in *Massive Neutrinos in Astrophysics and in Particle Physics*, edited by J. Tran Thanh Van (Editions Frontieres, Gif-sur-Yvette, France, 1984), p. 253.

[12] K. R. Hoffman, M. S. Dababneh, Y.-F. Hsieh, W. E. Kauppila, V. Pol, J. H. Smart, and T. S. Stein, Phys. Rev. A **25**, 1393 (1982).

[13] S. Zhou, Ph.D. dissertation, Wayne State University, 1993.

[14] H. S. W. Massey, Phys. Today **29** (3), 42 (1976).

[15] K. Higgins, P. G. Burke, and H. R. J. Walters, J. Phys. B **23**, 1345 (1990).

[16] H. R. J. Walters, J. Phys. B **21**, 1893 (1988).

[17] J. R. Winick and W. P. Reinhardt, Phys. Rev. A **18**, 910 (1978).

[18] J. R. Winick and W. P. Reinhardt, Phys. Rev. A **18**, 925 (1978).

[19] C. J. Brown and J. W. Humberston, J. Phys. B **18**, L401 (1985).

[20] J. Mitroy, J. Phys. B **29**, L263 (1996).

[21] A. A. Kernoghan, D. J. R. Robinson, M. T. McAlinden, and H. R. J. Walters, J. Phys. B **29**, 2089 (1996).

[22] F. J. de Heer, M. R. C. McDowell, and R. W. Wagenaar, J. Phys. B **10**, 1945 (1977).

[23] I. Bray, D. A. Konovalov, and I. E. McCarthy, Phys. Rev. A **43**, 5878 (1991).

[24] I. Bray, D. A. Konovalov, and I. E. McCarthy, Phys. Rev. A **44**, 5586 (1991).

[25] J. Callaway and K. Unnikrishnan, Phys. Rev. A **48**, 4292 (1993).

[26] W. L. van Wyngaarden and H. R. J. Walters, J. Phys. B **19**, 929 (1986).

[27] D. P. Dewangan, J. Phys. B **13**, L595 (1980).

[28] H. R. J. Walters, Phys. Rep. **116**, 1 (1984).

[29] F. W. Byron, Jr., C. J. Joachain, and R. M. Potvliege, J. Phys. B **15**, 3915 (1982).

[30] L. S. Fornari, L. M. Diana, and P. G. Coleman, Phys. Rev. Lett. **51**, 2276 (1983).

[31] L. M. Diana, P. G. Coleman, D. L. Brooks, P. K. Pendleton, and D. M. Norman, Phys. Rev. A **34**, 2731 (1986).

[32] D. Fromme, G. Kruse, W. Raith, and G. Sinapius, J. Phys. B **21**, L261 (1988).

[33] P. K. Biswas, M. Basu, A. S. Ghosh, and J. W. Darewych, J. Phys. B **24**, 3507 (1991).

[34] A. Ray, P. P. Ray, and B. C. Saha, J. Phys. B **13**, 4509 (1980).

[35] A. Igarashi and N. Toshima, Phys. Rev. A **50**, 232 (1994).

[36] K. Higgins and P. G. Burke, J. Phys. B **26**, 4269 (1993).

[37] R. J. Drachman and K. Omidvar, Phys. Rev. A **14**, 100 (1976).

[38] J. C. Straton, Phys. Rev. A **35**, 3725 (1987).

[39] D. Basu, G. Banerji, and A. S. Ghosh, Phys. Rev. A **13**, 1381 (1976).

[40] H. S. W. Massey and C. B. O. Mohr, Proc. Phys. Soc. London, Sect. A **67**, 695 (1954).

[41] W. C. Fon, K. A. Berrington, P. G. Burke, and A. E. Kingston, J. Phys. B **14**, 1041 (1981).

[42] J. S. Nico, D. W. Gidley, A. Rich, and P. W. Zitzewitz, Phys. Rev. Lett. **65**, 1344 (1990).